Elucidating interprotein energy transfer dynamics within the antenna network from purple bacteria

Dihao Wang, Olivia Fiebig, Dvir Harris, Hila Toporik, Yi Ji, Chern Chuang, Muath Nairat, Ashley Tong, John Ogren, Stephanie Hart, et al.

Elucidating inter-protein energy transfer dynamics within the antenna network from purple bacteria

Dihao Wang[a,1], Olivia C. Fiebig[a,1], Dvir Harris[a,1], Hila Toporik[b,c], Chern Chuang[a], Yi Ji[a], Muath Nairat[a], Ashley L. Tong[a], John I. Ogren[a], Stephanie M. Hart[a], Jianshu Cao[a], James Sturgis[d], Yuval Mazor[b,c], and Gabriela S. Schlau-Cohen[a,2]

[a]Department of Chemistry, Massachusetts Institute of Technology, Cambridge, Massachusetts 02139, United States; [b]School of Molecular Sciences, Arizona State University, Tempe, Arizona 85281, United States; [c]Biodesign Center for Applied Structural Discovery, Arizona State University, Tempe, Arizona 85281, United States; [d]LISM UMR 7255, CNRS and Aix-Marseille University, 31 Chemin Joseph Aiguier, Marseille Cedex 9 13402, France

This manuscript was compiled on January 21, 2022

Photosynthesis converts sunlight to chemical energy. In photosynthetic purple bacteria, absorbed light energy is first transferred within a network of antenna proteins, known as light-harvesting complex 2 (LH2), to reach the reaction center, which initiates the biochemical reactions. While the energy transfer dynamics of individual LH2 have been extensively studied over the past decades, the dynamics within the antenna network are poorly understood due to its heterogeneous and dynamic nature. Previously reported timescales were averaged over such heterogeneity, obfuscating individual LH2-to-LH2 energy transfer steps. Here, by embedding two LH2 into a near-native membrane disc, known as a nanodisc, we isolate and interrogate the organization and dynamics of protein pairs. We integrate ultrafast broadband transient absorption spectroscopy with cryo-EM microscopy to find an inter-protein energy transfer of 5.7 ps across 25 Å, which is the typical distance between neighboring LH2 in the membrane. The measured timescale represents the fast energy transfer between protein pairs in the antenna network, and simulations show these fast energy transfer steps can increase transport distances by 50% Overall, our results introduce a framework for well-controlled studies of inter-protein energy transfer dynamics, and suggest the closely-packed protein pairs serve as the primary pathway for LH2-to-LH2 energy transfer.

energy transfer | antenna network | nanodisc | femtosecond spectroscopy| cryo-EM |

Photosynthesis converts light energy to chemical energy to support nearly all life on Earth with a remarkable near-unity quantum efficiency (1–5). The high efficiency is achieved through a network of antenna proteins that absorb sunlight and then rapidly transport the resultant photoenergy over distances of 25-200 nm to reach reaction centers for charge separation. While nanometer-scale energy transfer within individual antenna proteins has been extensively characterized (3, 6–21), energy transport on the tens to hundreds of nanometer distances relies on inter-protein energy transfer. However, these energy transfer steps have been more challenging to probe due to the number of proteins involved, their heterogeneous organization, and their overlapping spectral features (22–25). As a result, many open questions remain about inter-protein energy transfer and how it gives rise to efficient yet long distance energy transport.

Purple bacteria are one of the most efficient classes of photosynthetic organisms and serve as model organisms for studies of photosynthetic light harvesting due to their well separated spectral features (26). Their primary antenna protein, light-harvesting complex 2 (LH2) or the B800-850 complex, is formed from subunits that assemble into an octameric, nonameric, or decameric cylindrical structure (24, 27–29). Each subunit binds one carotenoid and three bacteriochlorophyll a (BChla), which form two concentric rings upon assembly. One of the rings, denoted B800, consists of one BChla from each subunit and absorbs at 800 nm whereas the other, denoted B850, consists of two BChla from each subunit and usually absorbs at 850 nm (30–33). While these absorption features are typically observed, in some species the B850 ring blue-shifts to 820 nm under stress conditions due to a single amino acid substitution that restructures the hydrogen bonding network between the protein and the BChlas (30, 34, 35). This low-light variant of LH2 is known as LH3 or the B800-820 complex (31, 36). For all variants, energy rapidly transfers from the B800 to the B850 ring and around the B850 ring (3, 6–20, 30, 37–42).

After absorption and relaxation within LH2, energy transfers between the LH2 to reach light-harvesting complex 1 (LH1), which encircles the bacterial reaction center (RC) (3, 30, 37, 38, 43, 44). LH2 and LH1-RC are held together in the photosynthetic membrane in heterogeneous organizations

Significance Statement

Purple bacteria are one of the most ancient photosynthetic organisms and have evolved to perform light harvesting with near 100% quantum efficiency. Their high efficiency is achieved through rapid and efficient transport of absorbed solar energy across multiple light-harvesting proteins to reach the reaction center. Therefore, transport over long distances with high efficiency is a critical design parameter of photosynthetic light harvesting. Understanding this parameter requires that the dynamics and mechanism of energy transfer between light-harvesting proteins be resolved, but this crucial step has been experimentally inaccessible. Here, we incorporated two light-harvesting complexes from *Phaeospirillum molischianum*, LH2 and LH3, together into a near-native membrane disc and characterized their structural organization and energy transfer, identifying rapid energy transfer between the protein pairs. Corresponding simulations revealed the fast transfer within these pairs can enhance energy transport distances by 50%, pointing to these pairwise interactions as a key mediator of long distance energy transport.

Author contributions: G.S.S.-C. designed research; D.W., O.C.F., D.H., H.T., C.C., Y.J., M.N., A.L.T., J.I.O., and S.M.H. performed research; D.W., O.C.F., D.H., H.T., C.C., Y.J., J.C., J.S., Y.M., and G.S.S.-C. analyzed data; and D.W., O.C.F., D.H., C.C., Y.J., J.C., J.S., Y.M., and G.S.S.-C. wrote the paper.

The authors declare no competing interest.

[1]D.W., O.C.F., and D.H. contributed equally to this work.

[2]To whom correspondence should be addressed. E-mail: gssc@mit.edu

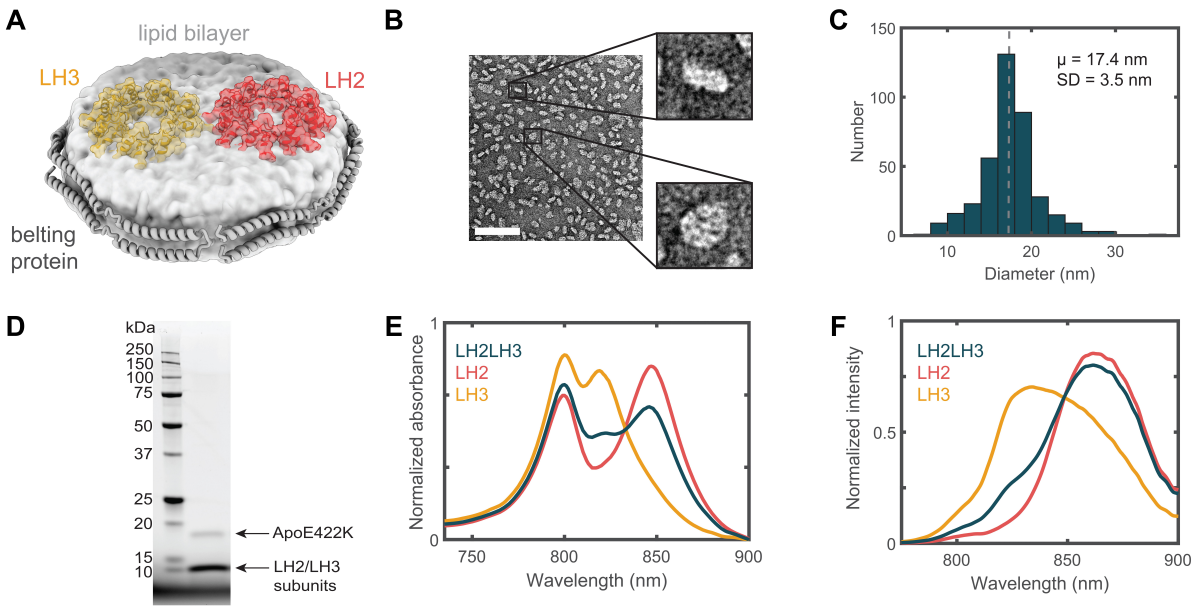

Fig. 1. Characterization of LH2-LH3 DLDs. (A) Cartoon image of LH2 (red) and LH3 (orange) embedded in a nanodisc. The lipid bilayer (light gray) is held together by ApoE422K belting protein (gray ribbons). (B) TEM image of nanodiscs. The scale bar (white line) is 100 nm. (C) Histogram of nanodisc size distribution from TEM images. The nanodiscs are 17.4 ± 3.5 nm in diameter. (D) SDS PAGE of nanodisc sample showing belting protein and LH2 and LH3 subunits. (E) Linear absorption spectrum of doubly-loaded LH2 (red), LH3 (orange), and LH2-LH3 (cyan) nanodiscs in the near-infrared region. The spectra are normalized by area. (F) Fluorescence spectrum of doubly-loaded LH2 (red), LH3 (orange), and LH2/LH3 (cyan) nanodiscs excited at 532 nm. The spectra are normalized by area.

and protein ratios, which further vary with growth conditions (5, 25, 34). To understand the energy transfer dynamics within the protein network, energy transfer timescales between LH2 and between LH1 and LH2 have been measured. Timescales of 2-10 ps were determined for LH2 to LH1 energy transfer (11, 30, 37, 45–47) and ∼5 ps for LH2-to-LH2 energy transfer (48). However, because LH2-to-LH2 energy transfer does not have any associated spectral changes, the timescale of this step was only indirectly resolved. Furthermore, these measurements were performed *in vivo* or on isolated membrane segments, which exhibit significant heterogeneity in the inter-protein distances. Energy transfer is expected to depend sensitively on the inter-protein distance, and so the reported values likely represent averages over a range of underlying timescales. Therefore, the specific timescales for protein-to-protein energy transfer have not yet been measured, despite their key role in long distance energy transport.

In this work, we isolate and interrogate energy transfer between LH2 variants by reconstituting LH2 and LH3 from *Phaeospirillum (Ph.) molischianum* together within a discoidal model membrane, known as a nanodisc (Fig. 1A), and measuring the LH3-to-LH2 energy transfer timescale within the nanodiscs. Nanodiscs are self-assembled discoidal lipid bilayers with well-controlled diameters and protein composition, and thereby provide a near-physiological yet homogeneous membrane-protein system (49–51). Using cryogenic electron microscopy (cryoEM), we characterized the structural organization of the LH2 variants within the nanodiscs and find that the closest distance between the low energy BChlas is ∼25 Å which is the canonical distance between neighboring LH2s within the native photosynthetic membrane, *in vivo*. (22, 52–54). Using transient absorption (TA) spectroscopy, we measured the LH3-to-LH2 energy transfer timescale and find a value of 5.7 ps. Supporting simulations emphasize that these protein pairs play an important role in achieving long-distance energy transport, effectively creating a super-highway for energy migration. Overall, these results determine the timescale for this critical energy transfer step and establish the utility of nanodiscs as a platform for bottom-up investigation of the photosynthetic antenna network.

Results and Discussion

LH2 variants in doubly-loaded membrane discs. To isolate and investigate energy transfer between LH2 proteins, we constructed doubly-loaded nanodiscs (DLD) with both LH2 and LH3 incorporated as illustrated in Fig. 1A. Nanodiscs are self-assembled discoidal membranes encircled by a stabilizing belting protein. The membrane composition and size depends on the ratios of the constituent lipids, membrane proteins, and belting proteins in the initial mixture. By varying the stoichiometry of the mixture, the discs were optimized for two LH2 per disc with a diameter sufficient to accommodate both complexes. Successful incorporation of LH2 into discs was suggested by SDS-PAGE of the purified DLD samples showing both LH monomer subunits and the belting protein, ApoE422K (Fig. 1B). Transmission electron microscopy analysis of the DLDs revealed discoidal structures with an apparent diameter of 17.4±3.5nm (Fig. 1C,D), confirming disc formation.

The integrity of the LH2 variants within the discs was confirmed by steady-state linear absorption and fluorescence spectra (Fig. 1E,F) for three DLDs samples: with LH2 only

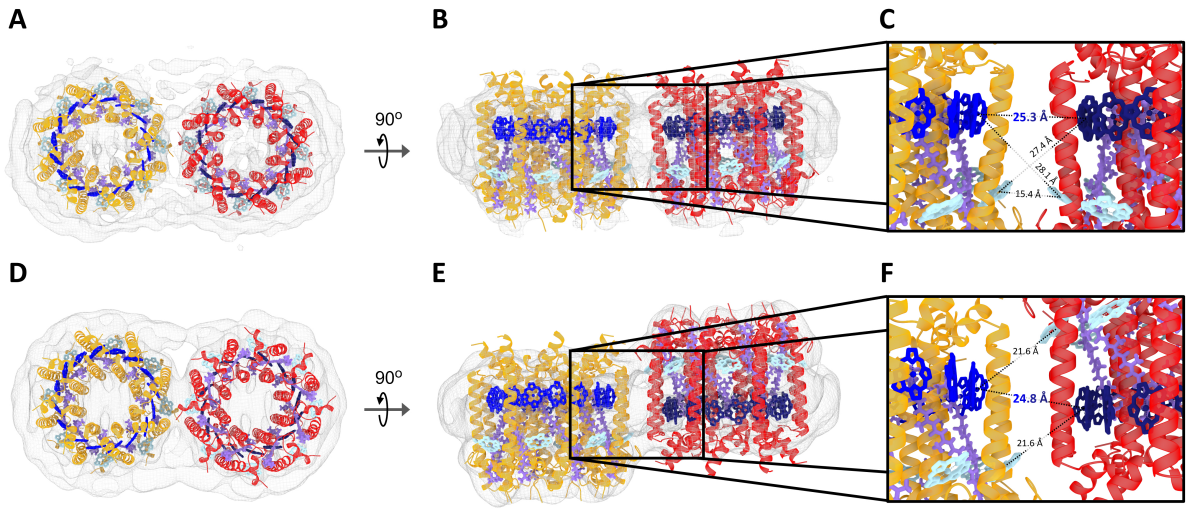

Fig. 2. Structural organization of LH2 variants in nanodiscs. CryoEM analysis of LH2-LH3 DLDs showing the electron density (light gray) and the docked structures (LH3 helices, orange; LH2 helices, red; B800 BChla, light blue; B850 BChla, dark blue; lycopene, purple). Two orientations, "parallel" (top row) and "anti-parallel" (bottom row), were observed. Top views of both orientations (A,D) illustrate the DLD assembly with the electron densities of belting proteins encircling the two LH proteins. Side views illustrate that the two LH2 are at the same approximate vertical position within the lipid bilayer for the parallel orientation (B) and are displaced vertically for the anti-parallel orientation (E). Both orientations reveal closely packed proteins with ∼25 Å between the BChla of the B820 and B850 rings.

(LH2 DLDs), LH3 (LH3 DLDs), and the LH2-LH3 mixture (LH2-LH3 DLDs). The overall peak profiles are similar to the proteins in detergent. For LH2 DLDs, the maximum of the B850 band red-shifted from 846 to 849 nm upon incorporation into the lipid bilayer, consistent with previous reports (9, 10). Similarly, for LH3 DLDs, the maximum of the B820 band red-shifted from 817 nm to 819 nm upon incorporation into the bilayer. The red tail of the B820 band for LH3 DLDs is due to a contribution of 5-10% LH2 (Fig. S5), as full conversion has not been achieved in this species (10). For the LH2-LH3 DLDs, incorporation of both LH2 and LH3 into the discs was confirmed through the linear absorption spectrum of the purified sample, which was decomposed into a 60%/40% combination of the spectra of the two variants (Fig. 1E). Finally, co-mixture of LH2 and LH3 within nanodiscs was established through the fluorescence spectrum of the LH2-LH3 DLDs sample (Fig. 1F). For stochastic LH2 and LH3 insertion, the LH2-LH3 DLD samples contain a mixture of LH2 DLDs, LH3 DLDs, and LH2-LH3 DLDs. Decomposition of the fluorescence spectrum into those of the two individual variants showed a 31% increase in LH2 content, consistent with a contribution from LH3-to-LH2 energy transfer at the level expected for stochastic insertion. At the 50 μM concentration of the fluorescence measurement, the presence of inter-protein energy transfer strongly implies incorporation of LH2 and LH3 into the same disc.

Cryogenic electron microscopy of doubly-loaded nanodiscs. To determine the architecture of the proteins within the DLDs, we used cryogenic electron microscopy (CryoEM) to resolve the structure of the LH2-LH3 DLDs at a highest resolution of 6.5Å, as shown in Figure 2. The formation of the DLD was successfully observed in the electron density - The encircling belting protein with two embedded membrane proteins are distinctly visible. Each of the embedded proteins had an apparent diameter of 7.1 nm and a clear octameric symmetry, consistent with the crystal structure of LH2 (PDB Code 1LGH) and the homology model of LH3 from *Ph. molischianum*. These features were utilized to dock the two into the densities. The DLD diameter of 17.1 nm from the high-resolution CryoEM structure is also in good agreement with the TEM average diameter of 17.4 nm (Fig. 1D).

Interestingly, two types of structures emerged from the analysis. One is similar to the native arrangement in which the BChl bands of each LH protein face the same side of the lipid bilayer as the BChl bands of the neighboring protein (hereafter, "parallel") as shown in the top row of Fig. 2. The second is a non-native arrangement in which the BChl bands of each LH protein face the opposite side of the bilayer as the bands of the neighboring protein (hereafter, "anti-parallel") as shown in the bottom row of Fig. 2. Notably, the anti-parallel structure dominates our sample, accounting for ∼85% of total particles analyzed. In addition to the apparent flip in orientation, the anti-parallel structure also shows a vertical displacement between neighboring proteins of ∼12Å along the perpendicular axis to the membrane plane (Fig. 2B,E). As a result of this displacement, the two low energy bands in the anti-parallel structure remain at nearly identical distances between the closest inter-complex BChl pairs as in the parallel structure, with values of 24.8Å and 25.3Å, respectively. Both of these values are on par with the canonical LH2-LH2 literature distance measured by Atomic force microscopy (AFM) (24, 54, 55), thus indicating the biologically-relevant distance was probed. Theoretical calculations (Table S5) show that the similar distances yielded energy transfer timescales within error, suggesting that the presence of two structures does not impact the measurements of inter-protein energy transfer.

Inter-protein energy transfer between LH2 variants. To probe the timescale of LH3-to-LH2 energy transfer, spectrally-resolved TA spectroscopy was performed on the DLDs with both LH2 and LH3 as shown in Fig. 3A. In order to accurately extract the inter-protein energy transfer timescale, LH2 DLDs and LH3 DLDs were also measured (Figs. S12 and S13). The spectral and temporal evolution of the TA data from all three samples was fit, where the values from the LH2 DLDs and LH3 DLDs were taken as fixed values for the LH2-LH3 DLDs data.

Both individual protein samples, the LH2 DLDs and LH3 DLDs, were fit using global analysis, which identifies the characteristic time constants and their associated spectral profiles, known as species-associated-decay-spectra (SADS) (56). The data was best fit with a sequential model in which the system evolves through three components. The first component decayed on a sub-picosecond timescale (850 fs for LH2-DLDs; 680 fs for LH3-DLDs) and the SADS was dominated by negative peak at ∼810 nm from the ground state bleach (GSB)/stimulated emission (SE) of the B800 band. Therefore, this component was assigned to B800 to B820/B850 energy transfer. Consistent with this assignment, the SADS associated with the second component were dominated by a negative peak at ∼860 nm for LH2 and ∼840 nm for LH3 from the GSB/SE of the B850 and B820 bands, respectively, as shown in Fig. 3C. A broad positive feature at higher energies (>850 nm for LH2 and >820 nm for LH3) was also present due to excited-state absorption (ESA) primarily from the B800 band. The timescale of the second component was 6.6 ps for LH2 DLDs and 8.1 ps for LH3 DLDs, and was assigned to vibrational relaxation. The final component exhibited a similar spectral profile and decayed on a ∼1.3 ns timescale, which is the approximate fluorescence lifetime of the LH2 variants. The time constants and their associated spectra are consistent with previous work (9, 10, 19, 39).

The spectra were also fit using a a three-step kinetic model in which, after photoexcitation of B800, (1) energy transfers from B800 to B850, (2) B850 undergoes vibrational relaxation, and (3) B850 relaxes to the ground state (SI Appendix, Fig. S9A). Single wavelength transients were taken at 2.5 nm intervals from 790 nm to 880 nm and globally fit to the kinetic model. The extracted time constants and spectral profiles were consistent with the components from the global analysis.

For the LH3-LH2 DLDs, LH3-to-LH2 energy transfer is also present. In the spectra from the LH2-LH3 DLDs, energy transfer can be observed. As shown in Fig. 3B, the GSB/SE signal at ∼830 nm from the B820 band decays with a corresponding rise in the GSB/SE signal at ∼860 nm from the B850 band. In order to extract the energy transfer time, the TA data was fit through the single wavelength kinetics, as the complexity of the data precluded direct fitting via global analysis. Due to the stochastic nature of the disc self-assembly process, the LH2-LH3 DLDs samples contain a mixture of LH2 DLDs, LH3 DLDs, and LH2-LH3 DLDs. Therefore, the

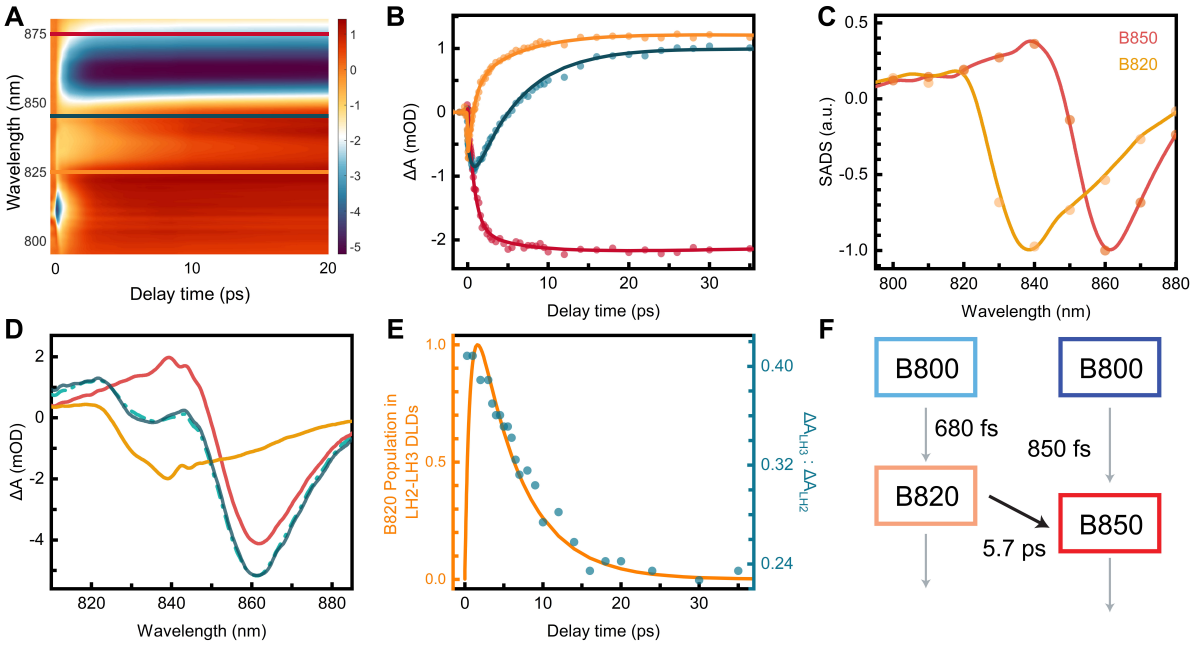

Fig. 3. LH3-to-LH2 energy transfer dynamics. (A) 2D representation of ultrafast TA spectra of LH3-LH2 DLDs. Color bar describes signal intensity (mOD). (B) Absorption transients of LH3-LH2 DLDs at wavelengths indicated in (A). Experimental values are shown as dots with fit values overlaid as solid lines. (C) SADS of B820 (orange) and B850 (red) extracted from the TA data of LH3 DLDs and LH2 DLDs, respectively. Results are shown from both simultaneous fitting of the single-wavelength kinetics (dots) and global analysis (lines). (D) Spectral decomposition of LH3-LH2 (dark green) TA difference spectrum at 5 ps time delay by LH2-LH2 and LH3-LH3 (red and yellow, respectively).The cyan dashed line is the simulated LH3-LH2 spectrum. (E) The relative changes in the coefficients (a/b) with time are in line with the population dynamics of B820 decay from the model fitting. (F) Schematic of the model used to fit the LH2-LH3 DLDs with values held fixed from LH2 DLDs and LH3 DLDs shown as gray arrows and the extracted LH3-to-LH2 energy transfer rate shown as a black arrow.

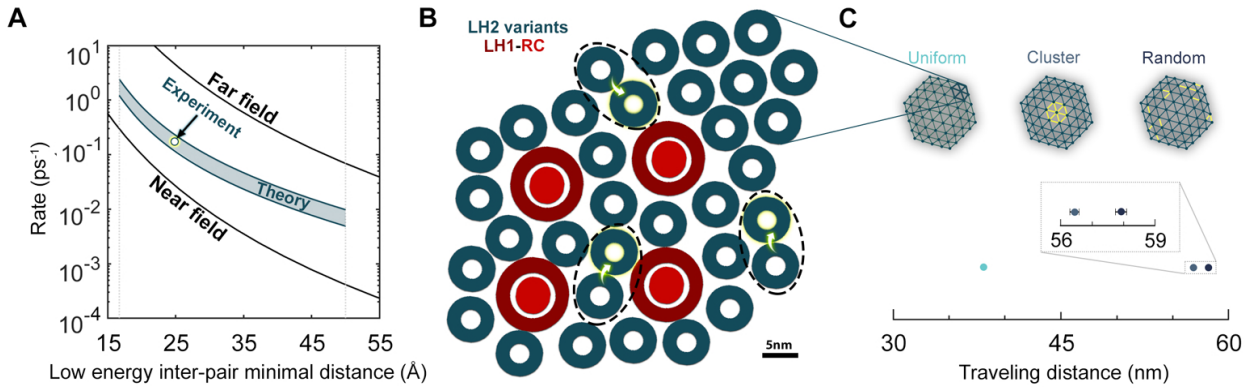

Fig. 4. Rate of LH3-to-LH2 energy transfer within the photosynthetic membrane (A)The inter-complex energy transfer rate as a function of the separation between the closest B820/B850 BChl pair. The dashed vertical gray lines define the biologically-relevant range of LH-LH distances based on AFM measurements of purple bacteria photosynthetic membranes (54, 55). The black lines represent far-field (top) and near-field (bottom) FRET regimes at R^{-6} scaling. The dark blue lines define a range of rescaled theoretical energy transfer rates such that the LH3-to-LH2 rate at the natural separation range is set to 0.1 ps^{-1} (bottom) and 0.2 ps^{-1} (top). The white dot represents the of experimental separation measured in the cryoEM structure and its appropriate experimental rate. (B) Schematic representation of *Ph. molischianum* photosynthetic membrane based on hrAFM (22) of this apparatus. Dotted oval containing naturally interacting LH3 and LH2. White arrows with yellow glow indicate energy transfer between the two. (C) The simulated effect of LH2 network distance heterogeneity on overall energy migration in hexagonal packing. Three setups (top, from left to right) - uniform, homogeneous spacing (4.8nm) of 156 inter-complex distances; 12 tightly interacting LH2-LH2 pairs (2.5nm) clustered in 144 loosely interacting (5nm) LH2-LH2 pairs; 12 tightly interacting LH2-LH2 pairs (2.5nm) randomly positioned with 144 loosely interacting (5nm) LH2-LH2 pairs. Migrated accumulated distance at 1ns time-frame for each configuration is shown (bottom) .

signal was fit to a sum of the evolution of the three samples described by kinetic models (SI Appendix, Fig. S9B). The intra-LH2 and intra-LH3 time constants and the SADS for all species were held fixed to the values determined through global fitting of the LH2 DLDs and the LH3 DLDs, leaving only the LH3-to-LH2 energy transfer time and the relative amplitudes for the samples as free parameters. LH3-to-LH2 energy transfer is most prominent within the spectral regions from 825 to 850 nm where the SADS of B820 and B850 have opposite signs (Fig. 3C). In this region, the negative signal becomes positive due to the decay of negative B820 and the rise of the positive B850 as illustrated in Fig. 3B. Therefore, transients within this spectral range were simultaneously fit in order to determine an LH3-to-LH2 energy transfer timescale of 5.7 ps.

To confirm LH3-to-LH2 energy transfer was successfully described by fitting to the kinetic model, the TA spectra from the LH2-LH3 DLDs were also decomposed into a linear combination of the LH2 and LH3 spectra. The relative contributions of the two spectra can be described by the ratio of LH3 to LH2 as shown in Fig. 3E. The ratio decreased with delay time in the LH2-LH3 DLDs consistent with LH3-to-LH2 energy transfer. In contrast, the ratio was nearly constant with delay time in a control sample of a simple mixture of LH2 and LH3 (Fig. S15C). The ratios from the LH2-LH3 DLDs are overlaid with the population dynamics of B820 from the model fitting. The evolution from both approaches shows good agreement, supporting the extracted timescale for energy transfer.

Förster theory calculations. The rate of LH3-to-LH2 energy transfer was also calculated using generalized Förster theory as shown in Fig. 4A. Generalized Förster theory describes the intermediate regime appropriate for photosynthetic light-harvesting apparatuses, *i.e.*, the inter-bacteriochlorophyll distances give rise to interactions between the far-field and near-field limits (57–60). For the ∼25 Å distance extracted from the CryoEM structures, the theoretical rate is 4.4 ps - 6.8 ps (see SI Appendix), similar to the experimental value of 5.7 ps. The good agreement between experiment and theory also illustrates that, even for inter-protein energy transfer, the far-field regime breaks down due the nanoscale distances involved.

Theoretical energy transfer timescales were also compared for LH3-to-LH2 and LH2-to-LH2 energy transfer (Table S5). Similar timescales and distance scaling were observed, confirming that LH3-to-LH2 energy transfer captures the behaviors associated with energy transfer amongst the LH2 variants in the membrane.

Energy transfer in the heterogeneous membrane. The LH3-to-LH2 timescale extracted from the LH3-LH2 DLDs corresponds to the canonical energy transfer between LH2 variants within the membrane, as the proteins are held together in a closely-packed organization through the facilitating nanoconfinement of the nanodisc. In AFM images of the photosynthetic membrane (22), instances of similar inter-protein distances were seen as illustrated in Fig. 4B. However, along with these closely-packed protein pairs, a range of other distances were observed within the heterogeneous protein network. In previous indirect measurements, an LH2-to-LH2 energy transfer timescale of ∼5 ps was found (48), similar to the 5.7 ps timescale extracted from the LH2-LH3 DLDs.

To investigate the importance of neighboring protein pairs in long distance energy migration, the energy transport dis-

tance was simulated using a hexagonal organization, which is a well established model for the arrangement of LH2 in the bacterial membrane (Fig. 4C) (61–63). The inter-protein distances were set to 2.5 nm and 5 nm, which is the canonical distance and the tail of the distance distribution observed in AFM measurements (54, 55). The covered distance was simulated for three different membrane arrangements: (i) equivalent inter-protein distances (4.8 nm); (ii) a protein cluster with distances of 2.5 nm and 5 nm within and without the cluster, respectively; and (iii) random distances of 2.5 nm within a lattice of 5 nm distances. In all arrangements, an average inter-protein distance of 4.8 nm was maintained.

As shown in Fig. 4, the simulations revealed a ∼70% increase in transport distances for the heterogeneous arrangements (ii, iii) over the equivalent arrangement (i). A small (∼2.5%) increase in transport distance was also observed for the random arrangement (iii) over the cluster (iii), suggesting no complex architecture is required. These results suggest that the local architecture of LH2-LH2 pairs within the photosynthetic membrane, and replicated using the nanodisc platform, provides an increased efficiency of energy transfer, and effectively creates a 'superhighway' for energy migration through the protein network.

Conclusion

In summary, we report isolation and characterization of the structure and dynamics of LH2 and its low-light variant LH3 from *Ph. molischianum*. Our results establish that nanodiscs, ultrafast TA spectroscopy, and cryoEM can, together, investigate inter-protein energy transfer of photosynthetic light harvesting.

Through this combination, we measured an inter-protein energy transfer timescale of ∼6 ps for the tightly-packed protein pairs, identifying the canonical inter-protein energy transfer within the protein network. Simulations and comparison to previous measurements suggests inter-protein energy transfer is dominated by these closely-packed protein pairs, which may be required for long distance energy transport. The ability of these protein pairs to dominate inter-protein energy transfer may also be a mechanism by which similar timescales are maintained despite heterogeneous protein organizations, allowing the light harvesting dynamics to be robust to the variations in antenna protein expression and organization used to adjust the light-harvesting machinery to the fluctuating conditions of natural environments.

Materials and Methods

Detailed description of the materials and methods is provided in the SI Appendix. This includes information on the sample preparation, cryo-EM procedures and structural determination, spectroscopic methods and data analysis, and details on the quantum chemical calculations.

ACKNOWLEDGMENTS. This work was supported by the U.S. Department of Energy, Office of Science, Office of Basic Energy Sciences, Division of Chemical Sciences, Geosciences, and Biosciences under Award DE-SC0018097 to G.S.S.-C. J.C. would like to acknowledge the National Science Foundation (CHE 1800301 and CHE 1836913). O.C.F. gratefully acknowledges support from an NSF Graduate Research Fellowship. D.H. would like to acknowledge the Yad Hanadiv (Rothschild) Foundation, the Zuckerman STEM Leadership Program, and the Israel Council for Higher Education (CHE) for their generous financial support. The authors thank Prof. Moungi Bawendi for the help with the near-infrared fluorescence measurements.

1. R. van Grondelle, J. P. Dekker, T. Gillbro, V. Sundström, Energy transfer and trapping in photosynthesis. *Biochim. Biophys. Acta* **1187**, 1–65 (1994).
2. T. Pullerits, V. Sündstrom, Photosynthetic light-harvesting pigment-protein complexes: Toward understanding how and why. *Acc. Chem. Res.* **29**, 381–389 (1996).
3. G. R. Fleming, R. van Grondelle, Femtosecond spectroscopy of photosynthetic light-harvesting systems. *Curr. Opin. Struct. Biol* **7**, 738–748 (1997).
4. T. Mirkovic, E. E. Ostroumov, J. M. Anna, R. van Grondelle, Govindjee, G. D. Scholes, Light absorption and energy transfer in the antenna complexes of photosynthetic organisms. *Chem. Rev.* **117**, 249–293 (2017).
5. X. Hu, T. Ritz, A. Damjanović, K. Schulten, Pigment organization and transfer of electronic excitation in the photosynthetic unit of purple bacteria. *J. Phys. Chem. B* **101**, 3854–3871 (1997).
6. V. Sundström, T. Pullerits, R. van Grondelle, Photosynthetic light-harvesting: Reconciling dynamics and structure of purple bacterial LH2 reveals function of photosynthetic unit. *J. Phys. Chem. B* **103**, 2327–2346 (1999).
7. R. Monshouwer, R. van Grondelle, Excitations and excitons in bacterial light-harvesting complexes. *Biochim. Biophys. Acta* **1275**, 70–75 (1996).
8. S. Hess, E. Akesson, R. J. Cogdell, T. Pullerits, V. Sundström, , Energy transfer in spectrally inhomogeneous light-harvesting pigment-protein complexes of purple bacteria. *Biophys. J.* **69**, 2211 (1995).
9. J. I. Ogren *et al.*, Impact of the lipid bilayer on energy transfer kinetics in the photosynthetic protein LH2. *Chem. Sci.* **9**, 3095–3104 (2018).
10. A. L. Tong *et al.*, Comparison of the energy transfer rates in structural and spectral variants of the B800-850 complex from purple bacteria. *J. Phys. Chem. B* **124**, 1460–1469 (2020).
11. S. Hess *et al.*, Temporally and spectrally resolved subpicosecond energy transfer within the peripheral antenna complex (LH2) and from LH2 to the core antenna complex in photosynthetic purple bacteria. *Proc. Natl. Acad. Sci. U.S.A.* **92**, 12333–12337 (1995).
12. S. Hess *et al.*, Femtosecond energy transfer within the LH2 peripheral antenna of the photosynthetic purple bacteria *Rhodobacter sphaeroides* and *Rhodopseudomonas palustris* LL. *Chem. Phys. Lett.* **216**, 247–257 (1993).
13. A. F. Fidler, V. P. Singh, P. D. Long, P. D. Dahlberg, G. S. Engel, Probing energy transfer events in the light harvesting complex 2 (LH2) of *Rhodobacter sphaeroides* with two-dimensional spectroscopy. *J. Chem. Phys.* **139**, 155101 (2013).
14. R. Jimenez, S. N. Dikshit, S. E. Bradforth, G. R. Fleming, Electronic excitation transfer in the LH2 complex of *Rhodobacter sphaeroides*. *J. Phys. Chem.* **100**, 6825–6834 (1996).
15. J. L. Herek *et al.*, B800→B850 energy transfer mechanism in bacterial LH2 complexes investigated by B800 pigment exchange. *Biophys. J.* **78**, 2590–2596 (2000).
16. T. Pullerits, S. Hess, S. J. L. Herek, V. Sundström, Temperature dependence of excitation transfer in LH2 of *Rhodobacter sphaeroides*. *J. Phys. Chem. B* **101**, 10560–10567 (1997).
17. T. Joo, Y. Jia, J.-Y. Yu,D. M. Jonas, G. R. Fleming, Dynamics in isolated bacterial light harvesting antenna (LH2) of *Rhodobacter sphaeroides* at room temperature. *J. Phys. Chem.* **100**, 2399–2409 (1996).
18. J. T. M. Kennis *et al.*, Femtosecond dynamics in isolated LH2 complexes of various species of purple bacteria. *J. Phys. Chem. B* **101**, 7827–7834 (1997).
19. J. A. Ihalainen *et al.*, Energy transfer in LH2 of *Rhodospirillum molischianum*, studied by subpicosecond spectroscopy and configuration interaction exciton calculations. *J. Phys. Chem. B* **105**, 9849–9856 (2001).
20. T. Pullerits M. Chachisvilis, V. Sundström, Exciton delocalization length in the B850 antenna of *Rhodobacter sphaeroides*. *J. Phys. Chem.* **100**, 10787–10792 (1996).
21. G. S. Schlau-Cohen, Q. Wang, J. Southall, R. J. Cogdell, W. E. Moerner, Single-molecule spectroscopy reveals photosynthetic LH2 complexes switch between emissive states. *Proc. Natl. Acad. Sci. U.S.A.* **110**, 10899–10903 (2013).
22. S. Scheuring, J. N. Sturgis, Chromatic adaptation of photosynthetic membranes. *Science* **309**, 484–487 (2005).
23. S. Scheuring *et al.*, Nanodissection and high-resolution imaging of the *Rhodopseudomonas viridis* photosynthetic core complex in native membranes by AFM. *Proc. Natl. Acad. Sci. U.S.A.* **100**, 1690–1693 (2003).
24. S. Scheuring, J.-L. Rigaud, J. N. Sturgis, Variable LH2 stoichiometry and core clustering in native membranes of *Rhodospirillum photometricum*. *EMBO J.* **23**, 4127–4133 (2004).
25. R. N. Frese *et al.*, The long-range organization of a native photosynthetic membrane. *Proc. Natl. Acad. Sci. U.S.A.* **101**, 17994–17999 (2004).
26. R. E. Blankenship *et al.*, Comparing photosynthetic and photovoltaic efficiencies and recognizing the potential for improvement. *Science* **332**, 805–809 (2011).
27. R. J. Cogdell *et al.*, The structural basis of light-harvesting in purple bacteria. *FEBS Lett.* **555**, 35–39 (2003).
28. S. Bahatyrova *et al.*, The native architecture of a photosynthetic membrane. *Nature* **430**, 1058–1062 (2004).
29. R. J. Cogdell *et al.*, The structure and function of the LH2 (B800-850) complex from the purple photosynthetic bacterium *Rhodopseudomonas acidophila* strain 10050. *Prog. Biophys. Mol. Biol.* **68**, 1–27 (1997).
30. R. J. Cogdell, A. Gall, J. Köhler, The architecture and function of the light-harvesting apparatus of purple bacteria: From single molecules to *in vivo* membranes. *Q. Rev. Biophys.* **39**, 227–324 (2006).
31. K. McLuskey, S. M. Prince, R. J. Cogdell, N. W. Isaacs, The crystallographic structure of the B800-820 LH3 light-harvesting complex from the purple bacteria *Rhodopseudomonas acidophila* strain 7050. *Biochemistry* **40**, 8783–8789 (2001).
32. J. Koepke, X. Hu, C. Muenke, K. Schulten, H. Michel, The crystal structure of the light-harvesting complex II (B800–850) from *Rhodospirillum molischianum*. *Structure* **4**, 581–597 (1996).
33. M. Z. Papiz, S. M. Prince, T. Howard, R. J. Cogdell, N. W. Isaacs, The structure and thermal

motion of the B800–850 LH2 complex from *Rps. acidophila* at 2.0 å resolution and 100 K: New structural features and functionally relevant motions. *J. Mol. Biol.* **326**, 1523–1538 (2003).
34. A. T. Gardiner, R. J. Cogdell, S. Takaichi, The effect of growth conditions on the light-harvesting apparatus in *Rhodopseudomonas acidophila*. *Photosynth. Res.* **38**, 159–167 (1993).
35. C. Mascle-Allemand, K. Duquesne, R. Lebrun, S. Scheuring, J. N. Sturgis, Antenna mixing in photosynthetic membranes from *Phaeospirillum molischianum*. *Proc. Natl. Acad. Sci. U.S.A.* **107**, 5357–5362 (2010).
36. J. Chmeliov *et al.*, Excitons in the LH3 complexes from purple bacteria. *J. Phys. Chem. B* **117**, 11058–11068 (2013).
37. Y. Yoneda *et al.*, Ultrafast photodynamics and quantitative evaluation of biohybrid photosynthetic antenna and reaction center complexes generating photocurrent. *J. Phys. Chem. C* **124**, 8605–8615 (2020).
38. F. Ma, L.-J. Yu, Z.-Y. Wang-Otomo, R. van Grondelle, Temperature dependent LH1→RC energy transfer in purple bacteria *Tch. tepidum* with shiftable LH1-Q_y band: A natural system to investigate thermally activated energy transfer in photosynthesis. *Biochim. Biophys. Acta* **1857**, 408–414 (2016).
39. M. Markus *et al.*, Low-intensity pump-probe measurements on the B800 band of *Rhodospirillum molischianum*. *Biophys. J.* **84**, 440–449 (2003).
40. G. D. Scholes, G. R. Fleming, On the mechanism of light harvesting in photosynthetic purple bacteria: B800 to B850 energy transfer. *J. Phys. Chem. B* **104**, 1854–1868 (2000).
41. Y. Saga *et al.*, Excitation energy transfer from bacteriochlorophyll b in the B800 site to B850 bacteriochlorophyll a in light-harvesting complex 2. *J. Phys. Chem. B* **125**, 2009–2017 (2021).
42. D. Zigmantas *et al.*, Two-dimensional electronic spectroscopy of the B800-B820 light-harvesting complex. *Proc. Natl. Acad. Sci. U.S.A.* **103**, 12672–12677 (2006).
43. F. Ma *et al.*, Excitation dynamics of two spectral forms of the core complexes from photosynthetic bacterium *Thermochromatium tepidum*. *Biophys. J.* **95**, 3349–3357 (2008).
44. G. S. Schlau-Cohen, E. De Re, R. J. Cogdell, G. R. Fleming, Determination of excited-state energies and dynamics in the B band of the bacterial reaction center with 2D electronic spectroscopy. *J. Phys. Chem. Lett.* **3**, 2487–2492 (2012).
45. F. G. Zhang, R. van Grondelle, V. Sundström, Pathways of energy flow through the light-harvesting antenna of the photosynthetic purple bacterium *Rhodobacter sphaeroides*. *Biophys. J.* **61**, 911–920 (1992).
46. V. Nagarajan, W. W. Parson, Excitation energy transfer between the B850 and B875 antenna complexes of *Rhodobacter sphaeroides*. *Biochemistry* **36**, 2300–2306 (1997).
47. L. Lüer *et al.*, Tracking energy transfer between light harvesting complex 2 and 1 in photosynthetic membranes grown under high and low illumination. *Proc. Natl. Acad. Sci. U.S.A.* **109**, 1473–1478 (2012).
48. R. Agarwal *et al.*, Nature of disorder and inter-complex energy transfer in LH2 at room temperature: A three pulse photon echo peak shift study. *J. Phys. Chem. A* **106**, 7573–7578 (2002).
49. I. G. Denisov, S. G. Sligar, Nanodiscs for structural and functional studies of membrane proteins. *Nat. Struct. Mol. Biol.* **23**, 481–486 (2016).
50. I. G. Denisov, S. G. Sligar, Nanodiscs in membrane biochemistry and biophysics. *Chem. Rev.* **117**, 4669–4713 (2017).
51. M. D. Hartley, P. E. Schneggenburger, B. Imperiali, Lipid bilayer nanodisc platform for investigating polyprenol-dependent enzyme interactions and activities. *Proc. Natl. Acad. Sci. U.S.A.* **110**, 20863–20870 (2013).
52. J. N. Sturgis, J. D. Tucker, J. D. Olsen, C. N. Hunter, R. A. Niederman, Atomic force microscopy studies of native photosynthetic membranes. *Biochemistry* **48**, 3679–3698 (2009).
53. J. D. Olsen *et al.*, The organization of LH2 complexes in membranes from *Rhodobacter sphaeroides*. *J. Biol. Chem.* **283**, 30772–30779 (2008).
54. R. P. Gonçalves, A. Bernadac, J. N. Sturgis, S. Scheuring, Architecture of the native photosynthetic apparatus of *Phaeospirillum molischianum*. *J. Struct. Biol.* **152**, 221–228 (2005).
55. S. Scheuring *et al.*, Watching the photosynthetic apparatus in native membranes. *Proc. Natl. Acad. Sci. U.S.A.* **101**, 11293–11297 (2004).
56. I. H. van Stokkum, D. S. Larsen, R. van Grondelle, Global and target analysis of time-resolved spectra. *Biochim. Biophys. Acta* **1657**, 82–104 (2004).
57. K. Mukai, S. Abe, H. Sumi, Theory of rapid excitation-energy transfer from B800 to optically-forbidden exciton states of B850 in the antenna system LH2 of photosynthetic purple bacteria. *J. Phys. Chem. B* **103**, 6096–6102 (1999).
58. H. Sumi, Theory on rates of excitation-energy transfer between molecular aggregates through distributed transition dipoles with application to the antenna system in bacterial photosynthesis. *J. Phys. Chem. B* **103**, 252–260 (1999).
59. L. Cleary, J. Cao, Optimal thermal bath for robust excitation energy transfer in disordered light-harvesting complex 2 of purple bacteria. *New J. Phys.* **15**, 125030 (2013).
60. J. Ma, J. Cao, Förster resonance energy transfer, absorption and emission spectra in multichromophoric systems. I. full cumulant expansions and system-bath entanglement. *J. Chem. Phys.* **142**, 094106 (2015).
61. T. J. Pflock *et al.*, The electronically excited states of LH2 complexes from *Rhodopseudomonas acidophila* strain 10050 studied by time-resolved spectroscopy and dynamic Monte Carlo simulations. II. Homo-arrays of LH2 complexes reconstituted into phospholipid model membranes. *J. Phys. Chem. B* **115**, 8821–8831 (2011).
62. M. Onizhuk, S. Sohoni, G. Galli, G. S. Engel, Spatial patterns of light-harvesting antenna complex arrangements tune the transfer-to-trap efficiency of excitons in purple bacteria. *J. Phys. Chem. Lett.* **12**, 6967–6973 (2021).
63. L. Cleary, H. Chen, C. Chern, R. J. Silbey, J. Cao, Optimal fold symmetry of LH2 rings on a photosynthetic membrane. *Proc. Natl. Acad. Sci. U.S.A.* **110**, 8537–8542 (2013).